Modeling an Injection Profile of Nanoparticles to Optimize Tumor Treatment Time with Magnetic Hyperthermia

Sonja Eagle, Samantha Wadsworth, Alexa Wnorowski

BEE 4530: Computer-Aided Engineering: Applications to Biomedical Processes
Spring 2015

Table of Contents

1.0 Executive Summary

Hyperthermia treatment to destroy cancerous tissue is a highly effective treatment strategy for malignant tumors. The goal of hyperthermia treatment is to raise the tumor temperature high enough to kill cancerous cells while minimizing damage to normal surrounding tissue. This project focuses on optimizing the treatment time using iron oxide magnetic nanoparticles (MNPs) to induce hyperthermia in cancerous tumors. In this treatment, the MNPs are injected into the center of the tumor, and their movement through the tissue is modeled using pressure-driven Darcy flow and simple mass diffusion. The MNPs are activated by a magnetic coil surrounding the tissue that produces an AC magnetic field, and heat is produced due to friction between the nanoparticles as they change orientation with the alternating current. This friction is sufficient to produce hyperthermia.

Because of the many parameters that can be changed in hyperthermia treatments, computational modeling of this process could provide a more efficient way of determining optimal treatments. However, most previous models do not model the injection and diffusion of nanoparticles, but rather have an exponential decay power equation as a heat source at the site of injection. To create a more accurate model, the injection process and mass diffusion of the nanoparticles can be modeled and coupled to the heating process through an electromagnetic heat source term.

In this COMSOL model, a tumor was approximated as a sphere surrounded by a sphere of normal tissue. Nanoparticle heat production within the tumor during exposure to a magnetic field is proportional to the nanoparticle concentration, which can be determined from the diffusion model including Darcy fluid flow. The transient temperature profile of the tissue was then monitored to observe the extent of damage to both the tumor tissue and surrounding healthy tissue. Treatment time was then optimized for a specific initial nanoparticle fluid concentration and injection velocity.

For a tumor with properties of a common liver tumor, nanoparticles with a concentration of 78600 g/m^3 were injected at a flow rate of 20 μL/min for fifteen minutes and allowed to diffuse for 24 hours. Under these conditions, optimal heating time was determined to be 11.5 minutes. In the future, this model could be adjusted based on tumor size, geometry, and specific parameters such as density, as well as various types of nanoparticles, and used in a clinical setting to determine optimal treatment prior to beginning the hyperthermia treatment.

2.0 Introduction, Background and Literature Review

Naturally, hyperthermia occurs when the body's thermoregulatory system fails, resulting in the overheating of body tissue, which is a medical emergency that can lead to severe tissue damage or death. However, in controlled situations, hyperthermia can be used as a therapy for treatment of diseases such as solid cancers. The temperature increase can be limited to a specific region so that the tumor tissue is damaged or destroyed, while damage to normal tissue is minimized[1].

There are several different techniques to induce hyperthermia for treatment of tumors, including ultrasound, lasers, and heating of magnetic nanoparticles (MNPs). Normally, treatments occur at temperatures in the range of 40-50ºC for anywhere from two minutes to several hours, depending on heating ranges desired[1-7]. For higher heating ranges, magnetic field amplitude and frequency can be altered to more powerful settings, which usually requires short treatment times; more mild heating ranges require lower powered magnetic fields and longer heating times[5, 7]. Mild hyperthermia treatments (40-43ºC) induce heat shock, and cause changes in the cell cycle that lead to faster denaturation of the pathogenic cells, and therefore faster cell death when exposed to radiation[8]. However, temperatures of 43ºC and above allow for necrosis, or direct cell death, which adds the benefit of fully killing some tumor tissue as opposed only destroying it[8]. Temperatures above 50ºC cause coagulation, temperatures of 60-90ºC result in thermoablation, and anything around 200ºC results in tissue charring[9]. Even if the tumors are not raised to temperatures of necrosis and fully destroyed, shrinking tumor size and damaging a maximum amount of tumor tissue is important for proceeding successfully with radiation therapy or chemotherapy, which almost always follows nanoparticle fluid hyperthermia treatment[9]. It has also been shown clinically in various animal species, as well as humans, that hyperthermia in the typical therapeutic range in combination with chemotherapy led to higher levels of survival than either treatment alone[10,11].

Magnetic fluid hyperthermia has proved challenging in vivo due to an inability to accurately determine temperature distribution and therefore obtain uniform and controlled heating. Advantages of MNP hyperthermia treatment include its minimal invasiveness and ability to specifically target cancerous tissue. For further advancement of this technique, computerized modeling is ideal[12].

Difficulties with MNP hyperthermia treatment for tumors include varying levels of blood perfusion, which should be incorporated into the model for realistic results. Perfusion creates a counteractive cooling action to the heating of the tumor. Strong perfusion, causing thermal convection in organs like the lungs, liver and kidneys, decreases the specific energy absorption of the tumor, and lowers the tumor temperature[10].

There are many different types of magnetic nanoparticles, and recent literature has explored how they affect hyperthermia treatment of tumors extensively[1-7, 12-15]. Iron oxide-based MNPs, while not showing the highest heating performance, remain a favorite due to their lack of toxicity, and excellent biocompatibility [7, 12, 13]. Iron oxides can also be further metabolized by heme oxygenase-1, forming blood hemoglobin, which maintains iron cell homeostasis in cells[10]. An additional consideration in choosing MNP type is the Curie temperature, which when it is around therapeutic temperature range can show self-regulation, given that at the Curie temperature, the Ms of particles drops to zero, and heating stops[10]. This can prevent reaching thermo-ablation temperature levels, and damaging the normal tissue. MNPs that have Curie temperatures near 45°C include $Fe_{27}Pt_{73}$ and $Ni_{28}Pd_{72}$, but their biocompatibility is not as promising[10]. For the AC magnetic field, researchers have generally focused pulsed frequencies in the range of 50kHz to 10MHz and magnetic field amplitudes in the range of 8-16 kA/m to achieve heating[2]. The most effective parameters reported by the year 2011 were a frequency of 500 kHz and a field amplitude of 10 kA/m[10].

Javidi et al. described a computational model of hyperthermia treatment using a homogenous distribution of iron oxide magnetic nanoparticles in an agarose gel[9]. Different agarose gel concentrations were used to model various potential pathogenic tissue densities, ranging from prostate tumors to brain tissue[12]. Varying injection velocities were also used in order to optimize heat generation while controlling overall temperature elevation[9]. This experimentally tested the distribution of nanoparticles that were injected into the agarose gel. It has also been previously shown that low injection flow rates aid in achieving a homogenous, spherical distribution of nanoparticles[12]. The nanoparticles were activated via an AC magnetic field with an amplitude and frequency of 1.2kA/m and 164kHz, respectfully[9]. Javidi and his team concluded that slower injection rates led to higher mean temperatures. This is due to a decreased dispersion of the nanoparticles, and therefore increased interactions between them. In addition, it was found that the lowest concentration of agarose gel density resulted in higher mean temperatures, due to decreased ability for the nanoparticles to move freely within the tissue. This indicates that while a localized high concentration of nanoparticles is favorable for higher heat production, the heat produced will most effectively spread through and therefore "treat" tumors with lower densities. This computational model was further verified experimentally.

3.0 Problem Statement

Magnetic fluid hyperthermia therapy can be used as a treatment for tumors. However, high temperatures induced by hyperthermia treatment can cause damage to surrounding cells. A COMSOL model of injection and diffusion of nanoparticles within a cancerous tumor, which couples the concentration profile to magnetic heating, can be used to optimize treatment time to maximize damage to tumor cells while minimizing damage to normal tissue.

4.0 Design Objectives

Design objectives were split into three parts:

1. Model the magnetic hyperthermia process by modeling particle injection, particle diffusion, and particle heating
2. Quantify the extent of tissue necrosis caused by the heating process
3. Optimize electromagnetic heating time to maximize tumor damage while minimizing damage to surrounding normal tissue based on specific tumor and nanoparticle properties.

5.0 Schematic

The process that was modeled is shown in Figure 1 below. A tumor is approximated as a sphere with a radius of r_i and is surrounded by a sphere of normal tissue with a radius of r_o. This geometric simplification was chosen because a sphere is a physically relevant approximation of how tumors grow in the body. Nanoparticles are injected through a needle at a depth of *b* below the top of the tumor. A

magnetic coil surrounds the tumor and provides the electromagnetic field necessary for the nanoparticles to heat the surrounding tissue.

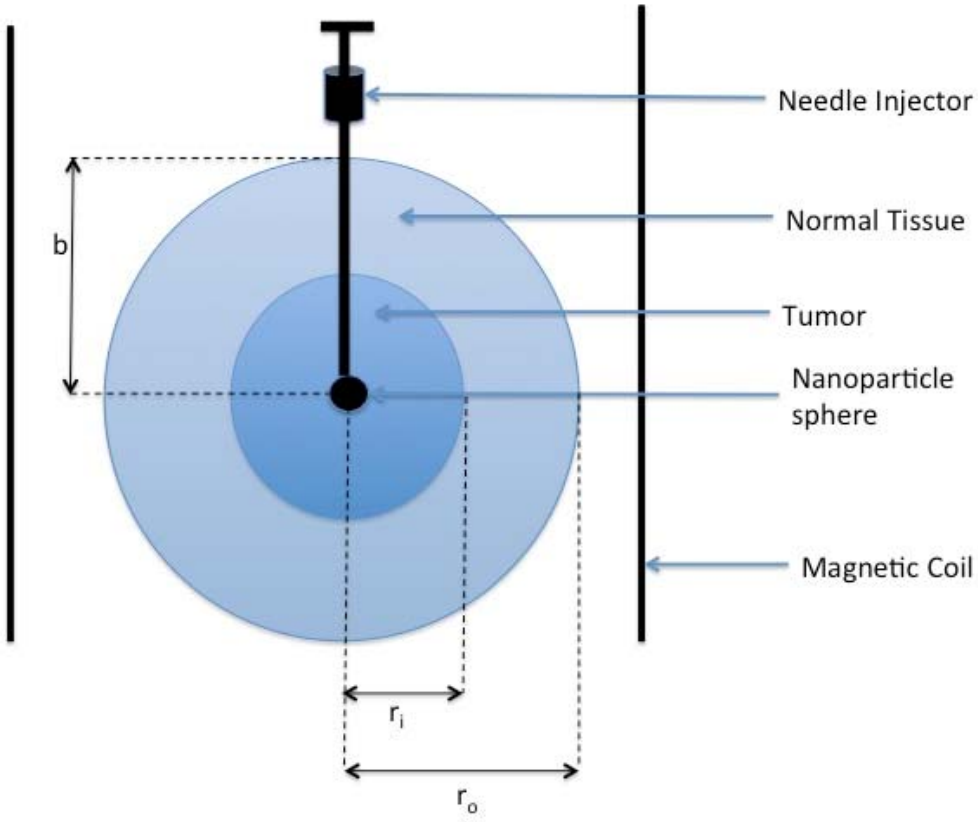

Figure 1. Schema of a 3D spherical tumor encased by a sphere of normal tissue, with a nanoparticle sphere injected into the center of the tumor. The entire tissue is surrounded by a magnetic coil.

For modeling purposes, this scenario was implemented in COMSOL as a 2D axisymmetric problem as shown in Figure 2 below. The tumor radius was set to r_i = 25.400 mm, with surrounding normal tissue with a radius of r_o = 50.000 mm. A 15-gauge needle was used because this is the standard size used for such injection procedures in humans[11]. This standard sized needle has an inner diameter of 1.372 mm (and therefore an inner radius of 0.686 mm). It was assumed to penetrate to the center of the tissue, and that when the needle was removed it left open space in the tissue. The penetration depth of the needle into the tissue *b* was assumed to be equal to the radius of the outer sphere so that the needle tip injected nanoparticle fluid into the center of the model. The magnetic nanoparticle fluid is injected downwards out of the needle tip.

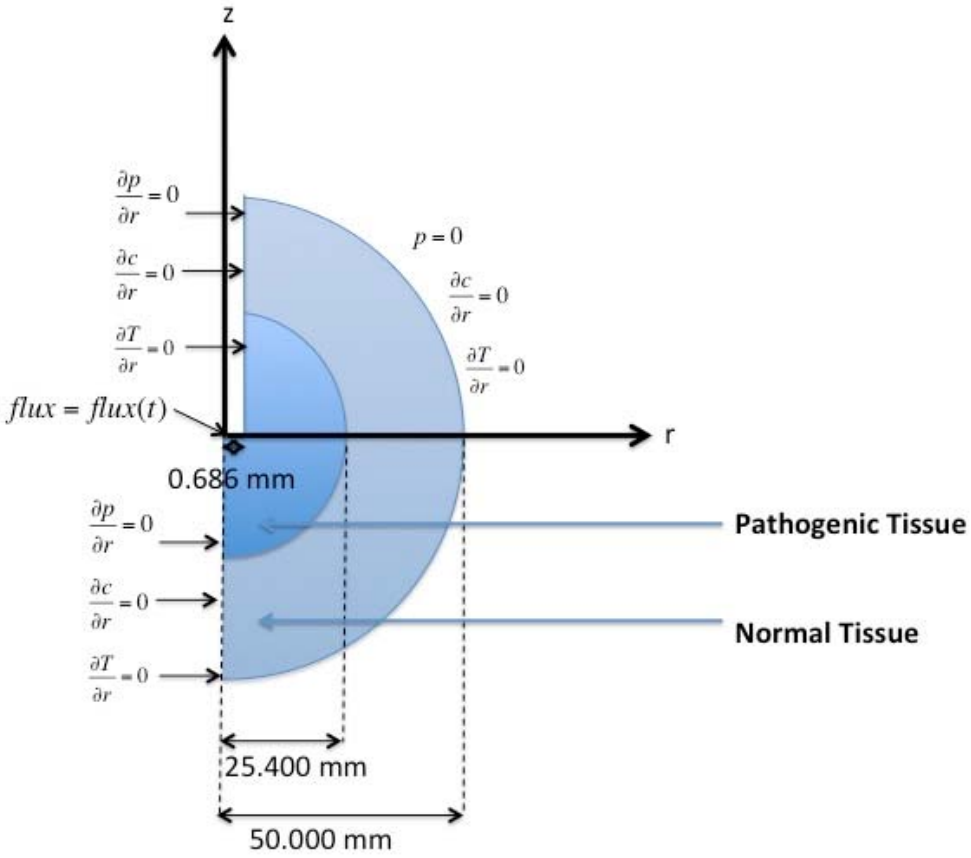

Figure 2. Schema of a 2D axisymmetric representation of a spherical tumor surrounded by normal tissue, with an injected 15 gauge needle (with an inner radius of 0.686 mm) in the center. Boundary conditions for the pressure-driven flow of nanoparticle fluid, mass transfer, and heat transfer processes are shown. The boundary at the tip of the needle is a flux boundary that is time dependent; there is a flux of 0.228138 kg/(m^2*sec) during the initial fifteen-minute injection period, after which it decreases to zero over 40 seconds and remains at zero for the rest of the computation.

6.0 Methods

The process of hyperthermia treatment for malignant tumors using magnetic nanoparticle therapy was modeled in four steps: (1) injection of the nanoparticle fluid through a needle using pressure-driven Darcy flow for 15 minutes; (2) mass diffusion of the magnetic nanoparticles into the tumor due to the injection pressure for 24 hours, (3) heat transfer from the magnetized nanoparticles into the tissue after nanoparticle dispersion into the tumor tissue and magnet activation for eleven minutes, and (4) quantification of the extent of tissue necrosis determined using the theory of cumulative equivalent minutes of heating at 43ºC. COMSOL was used to model these four processes. Once the model was developed, an optimization function could be used to determine optimal heating time based on the given input parameters.

In order to realistically model these three processes concurrently, they were set to occur at different times. At the starting time (t = 0 seconds), the injection pressure is applied for 15 minutes, and diffusion is allowed to occur for 24 hours after the start of injection, as per standard protocol for the treatment[3]. It is not until this time that the heating begins.

6.1 Implementation in COMSOL

The geometry described in Figure 2 was implemented into COMSOL as a 2D axisymmetric problem. The tumor and normal tissue were unified, following the assumption that the tumor tissue and normal tissue exhibit the same physical properties. The physics additions were (1) Darcy Flow, to describe the pressure driven flow out of the syringe, (2) Transport of Diluted Species, to describe the mass flow of the nanoparticle fluid out of the syringe and into the tissue, and (3) Heat Transfer in Solids, to describe heating of the tissue. These physics were run simultaneously to ultimately give a temperature profile of the tumor and surrounding tissue that was dependent on the injection velocity and resulting dispersion of the MNPs.

6.1.1 Darcy Flow

Pressure-driven fluid flow of the nanoparticle fluid out of the syringe tip is described by Darcy's Law:

$$\frac{\partial}{\partial t}\left(\rho\epsilon_p\right) + \nabla \cdot (\rho u) = 0 \quad (1)$$

$$u = -\frac{\kappa}{\mu}\nabla P \quad (2)$$

where ρ is the nanoparticle fluid density, ϵ_p is the tumor porosity, κ is the tumor permeability, and μ is the nanoparticle fluid dynamic viscosity. Fluid properties were approximated according to Table 1 of Appendix 9.2. Boundary conditions include pressure being equal to zero at the outer normal tissue boundaries because it is assumed far enough away from the nanoparticle injection site, pressure gradient being equal to zero at the lower left boundary (beneath the needle injection site) due to symmetry, and pressure gradient being equal to zero at the upper left boundary where the needle shaft contacts the tissue due to insulation.

A mass flux of 0.228238 kg/(m^2*s) was applied at the tip of the needle to model to injection of nanoparticle fluid into the tumor, which is equivalent to a volume flow rate of 20 μL/min[9]. This was calculated based on the fluid density and the needle tip area of a 15-guage needle as follows:

$$flux = \frac{(\rho_{fluid})(Q)}{A_{needle}}$$

$$flux = \frac{(1011.85\ kg/m^3)(20\mu L/min)}{\pi(.000686m)^2}$$

$$flux = 0.228138\ kg/(m^2 * s)$$

The fluid leaving the tip is at a concentration of 78,600 g nanoparticles/m^3, based on a volume fraction of 0.015[16]. Injection occurred for 15 minutes in order to inject 300 μL total[9] and then was allowed 40 seconds for the mass flux to linearly decrease to 0 kg/(m^2*s) for computational ease, and to take into account the withdrawal of the needle. The Darcy flow problem was then implemented in COMSOL, to solve for the velocity profile of the nanoparticles into the tumor that can be coupled to the nanoparticle mass transfer process.

6.1.2 Transport of Diluted Species

Mass transfer of the nanoparticles throughout the tissue after needle injection can be modeled as a transient process, with the governing equation simplifying to:

$$\frac{\partial c_{NP}}{\partial t} + u_r \frac{\partial c_{NP}}{\partial r} + u_z \frac{\partial c_{NP}}{\partial z} = D_{NP,tissue} \left[\frac{1}{r}\left(\frac{\partial}{\partial r} r \frac{\partial c_{NP}}{\partial r}\right) + \frac{\partial^2 c_{NP}}{\partial z^2}\right] \quad (3)$$

where c_{NP} is the nanoparticle concentration, $D_{NP,\,tissue}$ is the diffusivity of the nanoparticles through the tissue, and u is the convective velocity profile as defined by Darcy flow in section 6.1.1. Parameter values used are shown in Table 2 of Appendix 9.2. As there are no nanoparticles in the tumor or normal tissue before treatment, the initial concentration in these regions was defined as 0 g/m^3. However, for computational reasons this value was defined as "eps" in COMSOL (a figure that is essentially zero). Boundary conditions include mass flux being equal to zero at the far normal tissue boundary because it is considered far enough away, flux being equal to zero at the left lower boundary due to symmetry, and flux being equal to zero at the left upper boundary where the needle contacts the tissue due to insulation. In order to obtain the most effective heating process, diffusion was allowed to occur for 24 hours (or 86,400 seconds) after the start of injection before beginning heating.

6.1.3 Heat Transfer in Solids

After 24 hours of nanoparticle diffusion, the electromagnetic heat source was applied to begin heating. Tissue heating was described using the following governing equation:

$$\frac{\partial T}{\partial t} = \frac{k}{\rho c_p}\left[\frac{1}{r}\left(\frac{\partial}{\partial r} r \frac{\partial T}{\partial r}\right) + \frac{\partial^2 T}{\partial z^2}\right] + Q_b + Q_m \quad (4)$$

where ρ is the tissue density, c_p is the tissue specific heat, k is the tissue thermal conductivity, Q_b is bioheat generation, and Q_m is the magnetic heat generation from the nanoparticles.. This is a transient process that does not include the consideration of Darcy fluid flow because injection has stopped 24 hours before heating will begin. However, it is coupled to the mass diffusion process through the magnetic heat generation term, which is proportional to nanoparticle concentration.

Bioheat generation is the normal metabolic heat generation in body tissue. It can be described by:

$$Q_b = \rho_b c_{p,b} \dot{V}_b^v (T - T_a) \quad (5)$$

where ρ_b is blood density, $c_{p,b}$ is the blood specific heat, $\dot{V}_b^v$ is volume flow rate, and T_a is arterial blood temperature.

Power dissipation of the heat generated by the magnetic nanoparticles can be described as follows[9]:

$$Q_m = \pi\mu_0 x_o H_o^2 f \frac{2\pi f\tau}{1+(2\pi f\tau)^2} \tag{6}$$

where the effective relaxation time, τ, is described by:

$$\tau^{-1} = \tau_N^{-1} + \tau_B^{-1} \tag{7}$$

where τ_N and τ_B are the Neel and Brownian relaxation time respectively. They are calculated as follows:

$$\tau_N = \frac{\sqrt{\pi}}{2}\tau_o \frac{\exp(\Gamma)}{\sqrt{\Gamma}} \tag{8}$$

$$\tau_B = \frac{3\eta V_H}{kT} \tag{9}$$

where τ_o is the average relaxation time in response to thermal fluctuation, η is the viscosity of the MNP fluid, k is the Boltzmann constant, and T is temperature. The shorter time constant will dominate in determining the effective relaxation time.

V_H is the hydrodynamic volume of MNPs, determined by:

$$V_H = \frac{\pi(D+2\delta)^3}{6} \tag{10}$$

where D is the diameter of MNPs and δ is the ligand layer thickness.

Γ is a function determined by:

$$\Gamma = \frac{KV_M}{kT} \tag{11}$$

where K is the magnetocrystalline anisotropy constant and V_M is the volume of MNPs, defined by:

$$V_M = \frac{\pi D^3}{6} \tag{12}$$

The equilibrium susceptibility, x_o, is assumed to be the chord susceptibility, expressed as:

$$x_o = x_i \frac{3}{\xi}\left(\coth\xi - \frac{1}{\xi}\right) \tag{13}$$

where:

$$x_i = \frac{\mu_o \phi M_d^2 V_M}{3kT} \tag{14}$$

$$\xi = \frac{\mu_o M_d H V_M}{kT} \tag{15}$$

$$H = H_o \cos(\omega t) \tag{16}$$

where H_o is the amplitude of the magnetic field and ω is the angular frequency defined by:

$$\omega = 2\pi f \tag{17}$$

where f is frequency of the magnetic field. M_s and M_d are the saturation and domain magnetization respectively, and are proportional:

$$M_s = \phi M_d \tag{18}$$

where ϕ is the volume fraction of MNPs, defined by:

$$\phi = \frac{c_{NP}(r,\theta)}{\rho_{NP}} \tag{19}$$

The nanoparticle concentration, $c_{NP}(r,\theta)$, is obtained from the mass transport of nanoparticles described in Section 6.1.2 above. Parameter values used for heat transfer calculations are described and defined in Table 3 in Appendix 9.2.

Initially, the temperature of the entire domain was set to 37ºC (or 310.15K) to represent body temperature. For boundary conditions, mass and heat flux at the left and bottom boundaries are set to zero due to symmetry. The top and right boundaries can be assumed to be at a semi-infinite distance, so mass and heat flux would be zero at those boundaries as well. Heating was set to begin at the end of the 24-hour diffusion period, and the actual time of heating was left to be determined by optimization.

After all physics were implemented in COMSOL, a mesh was designated using COMSOL's built in physics-controlled option, at an extremely fine level with smaller elements along the needle tip and the tumor boundary on the axis. This mesh was determined based on the mesh convergence after 30 minutes of heating as shown in Appendix 9.1. This time was estimated as the maximum time that would be required to heat the tumor, given that our desired temperatures were in the range of hyperthermia that achieves necrosis, which require shorter treatment times than milder hyperthermia.

6.2 Model Optimization

One of the design aims of this model is to optimize heating time to obtain maximal tumor damage while minimizing normal tissue damage. In order to do this quantitatively, an objective function J was defined as:

$$J = \sum_i f_t(T_i) + \sum_j f_n(T_j) \tag{22}$$

where

$$f_t(T_i) = \begin{cases} 43 - T; & T < 43 \\ 0; & 43 \leq T \leq 50 \\ T - 50; & T > 50 \end{cases} \tag{23}$$

$$f_n(T_j) = \begin{cases} 37 - T; & T < 37 \\ 0; & 37 \leq T \leq 38 \\ T - 38; & T > 38 \end{cases} \tag{24}$$

This function sums up the objective function at all points *i* corresponding to the tumor temperature and all points *j* corresponding to the normal tissue temperature. The function will be optimized (be at its minimum value) when the temperature of the normal tissue is in the desired range of 37-38ºC (not deviating far from body temperature) and temperature of the tumor reaches the desired temperature range for necrosis to occur, or 43-50ºC[8,17]. At temperatures greater than 50ºC, coagulation occurs, between 60ºC and 90ºC cells thermoablate, and at temperatures greater than 200ºC, charring occurs[9]. Therefore, 50ºC was chosen as the upper temperature threshold for necrosis because it is desirable to achieve necrosis but not for temperatures to get so high that coagulation occurs. Additionally, 50ºC is the maximum temperature that can be reached while maintaining no damage to surrounding normal tissue[18]. Only a very small temperature range is tolerated for the normal tissue because it is more important to ensure that normal tissue is not damaged than it is for all of the tumor tissue to be destroyed and it should be ensured that normal tissue does not come close to the temperature required for necrosis. This objective function can be calculated for various heating times. The minimum value on a plot of objective function vs. heating time can then be used to determine the optimal heating time to give the desired conditions and implemented to obtain the final temperature profile described in Section 6.1.3.

6.3 Quantifying Tissue Necrosis

Using the resulting temperature profile of the tumor after heating, the extent of tissue damage (necrosis) can be determined. Because necrosis is a function of both temperature and time, data must be converted to a standard for comparison of different heating times and temperatures. One method proposed involves converting time-temperature data to an equivalent number of minutes at an index temperature of 43ºC[19]. The resulting data is indicative of how long that tissue has been at the equivalent of 43ºC. There was no particular reason for choosing 43ºC as the reference point (any temperature can be used theoretically)

aside from the fact that 43ºC is the breakpoint for several cell lines. The breakpoint is a reference point in the Arrhenius plot of 1/Do vs. 1/T, where Do is the number of minutes to reduce survival of cells 63%. Arrhenius plots are typically biphasic, with a steeper and then a more shallow portion, and the point where they switch is called the breakpoint. The breakpoint is consistent with the heat of inactivation of cells. The equation for this conversion is:

$$CEM43 = tR^{(43-T)} \tag{20}$$

where CEM43 is the cumulative number of equivalent minute at 43ºC, t is the time interval (minutes), and T is the average temperature during time interval t. R is the number of minutes needed to compensate for a 1 degree temperature change either above or below the breakpoint. For situations where the temperature is changing (i.e. when the tumor is heating up), CEM43 must be calculated for small sub-time intervals where the temperature is relatively constant, and then summed over the entire time interval to represent the entire exposure.

If the thermal dose to achieve necrosis is known for one time and temperature combination, equation 20 can be used to convert to required time at other temperatures. The R value will be different below and above the breakpoint, which has been empirically determined to be 43.5ºC in humans. Above the breakpoint, the rate of killing essentially doubles for every degree increase in temperature. The R value below the breakpoint is 0.233, and 0.428 above the breakpoint[17].

To account for varying temperature at different tissue locations, CEM43 must be integrated over the entire domain. Rewriting equation (20) in differential form gives:

$$\frac{dCEM43}{dt} = R^{(43-T)} \tag{21}$$

This process can be visualized by defining a new ordinary differential equation in COMSOL, with a reaction term equal to $R^{(43-T)}$. Necrosis occurs at 43ºC after heating for 340 minutes[20]. Therefore, tissue that had experienced enough heating to get it to the equivalent isoeffect of 340 minutes at 43ºC was considered to have undergone necrosis.

7.0 Results and Discussion

7.1. Mesh

In order to determine the optimal maximum element size, a mesh convergence was done as shown in Appendix 9.1. It was completed after calculating the nanoparticle concentration profile but before temperature calculations because the time of heating was not determined until the optimization step. The resulting mesh used the COMSOL extremely fine physics-controlled mesh option, as shown in Figure 3. This allowed for more sensitive calculations at the needle tip where the pressure gradient was largest due to injection where the pressure boundary was set, and less sensitive calculations at the edges of the tumor

and normal tissue. The default maximum element size of 0.0014 m was used, with smaller element size of 0.001m used along the needle tip and the axis of symmetry of the tumor below the needle.

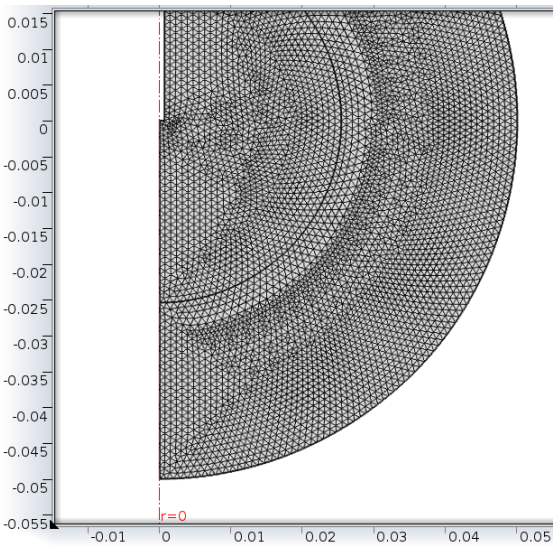

Figure 3: Schema of tumor tissue (inner circle) and normal tissue (outer circle), with a built-in COMSOL extremely fine physics-controlled mesh, with smaller elements along the needle tip and the tumor boundary on the axis. The mesh shows smaller units near the pressure boundary, allowing for more sensitive calculations at the injection site, and larger units at the edges of the tumor and tissue, where more sensitive calculations are not necessary. The mesh is the most fine around the needle tip area.

7.2 Injection

The injection, based on a mass flux of 0.228238 kg/(m^2*s) was applied for 15 minutes (900 seconds) and then removed over a period of 40 seconds, leaving a flux of 0 kg/(m^2*s) for the rest of the procedure. The injection process is shown in Figure 4.

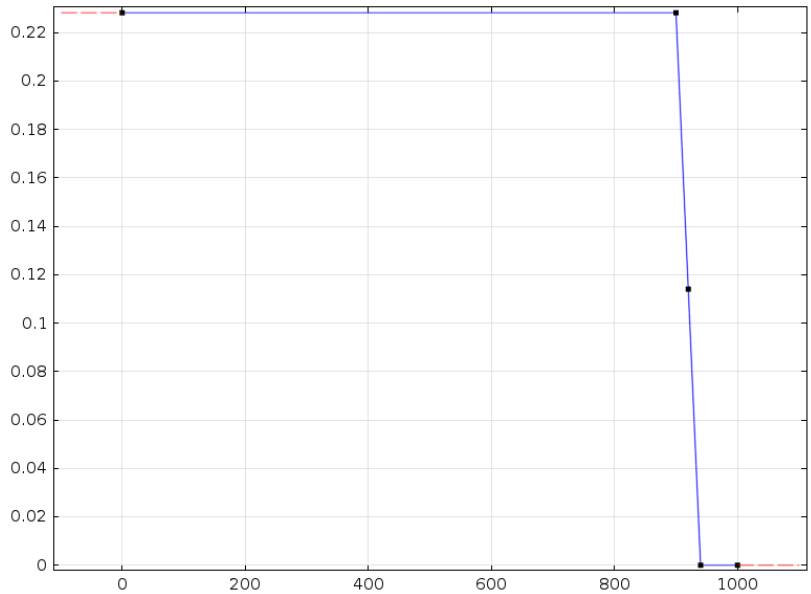

Figure 4: Mass flux (kg/(m^2*s)) vs. time (seconds) to show injection function for injection of nanoparticles at 78600 g/m^3 from a syringe with a 1.372 mm diameter needle tip.

The pressure within the tumor reached its highest point right at the 15 minutes, or the time at end of the injection. It then slowly diffused over the 24 hours before heating time, as seen in Figure 5.

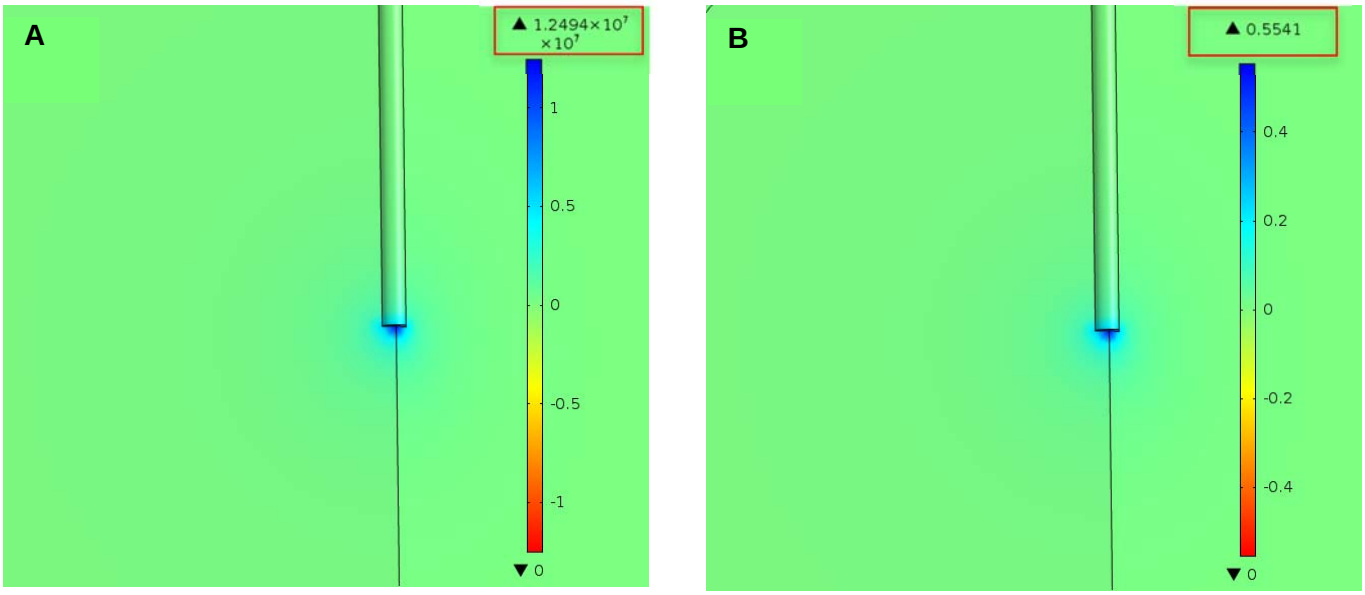

Figure 5: Pressure gradients at the needle tip at the center of the tumor, at (a) 900 seconds, corresponding to the end of the fifteen minute injection with a mass flux of 0.228238 kg/(m^2*s) and (b) 86,400 seconds, corresponding to the end of the 24 hour diffusion period before heating occurs. The maximum pressure achieved is 1.2494 x 10^{14} Pa after 15 minutes and 0.5541 Pa at the end of the 24 hour diffusion period.

Monitoring the pressure at the end of injection and at the end of the diffusion period confirmed that the mass flux boundary implemented to model the injection process was successful, and that injection comes to an end after 15 minutes.

7.3 Diffusion

At the end of the injection process, there is a high concentration of nanoparticles localized to the injection site. Twenty-four hours were given to allow these nanoparticles to diffuse out within the tumor. This diffusion process can be seen in Figure 6.

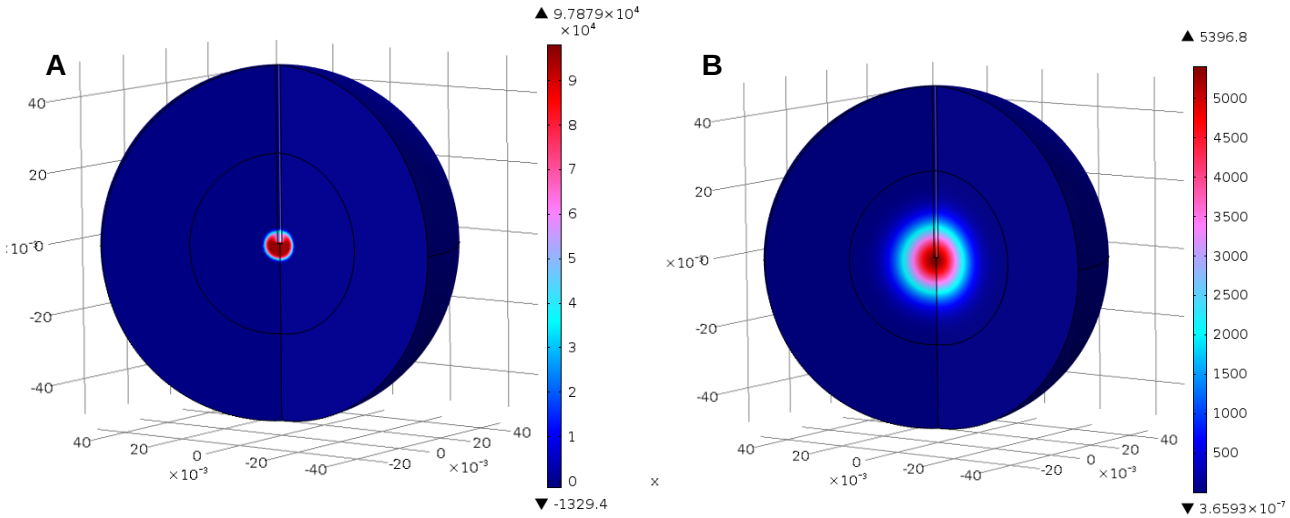

Figure 6: Concentration gradient in grams of nanoparticles within the tumor tissue, at (a) 900 seconds, corresponding to the end of the fifteen minute injection with a mass flux of 0.228238 kg/(m^2*s) and (b) 86,400 seconds, corresponding to the end of the 24 hour diffusion period before heating occurs.

As can be seen in Figure 6, the nanoparticles are highly concentrated and not widely dispersed after injection, and are less concentration but more disperse after 24 hours. This 24-hour diffusion period was necessary in order to ensure that the nanoparticles become sufficiently dispersed throughout the tissue so that heating occurred over a larger area of tumor tissue. Additionally, since temperature is proportional to nanoparticle concentration, allowing the concentration profile to become less concentrated helped ensure that the temperatures reached during heating were not too hot.

7.4 Optimization of Heating

Optimization was performed for heating times between ten and fifteen minutes, according to the optimization function (Equation 22). The function J was plotted versus heating time as shown in Figure 7. The function was created to be optimal when minimized, and thus the ideal heating time that maximizes necrosis and other damage of this tumor tissue while minimizing any damage to the normal surrounding tissue was 11.5 minutes. This was then implemented into the COMSOL as the time that the electromagnetic field was applied, giving a final model time of 87,090 seconds.

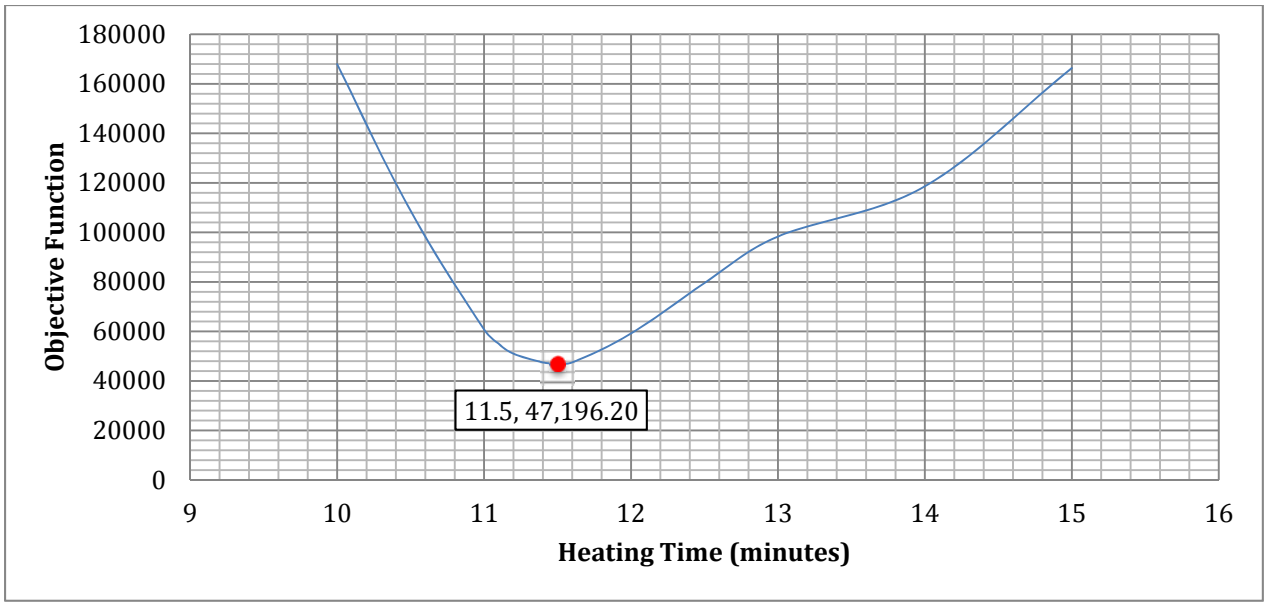

Figure 7. Objective function plotted versus heating time. The objective function was set up to minimize damage to normal tissue while maximizing necrosis of tumor tissue. Since the objective function reaches a minimum at approximately 11.5 minutes this is the ideal heating time.

This heating time maximized the amount of tumor tissue being heated between 43-50ºC and minimized any normal tissue heating to over 38ºC. Figure 8 shows a surface plot of optimization function values over the entire domain at 11.5 minutes of heating.

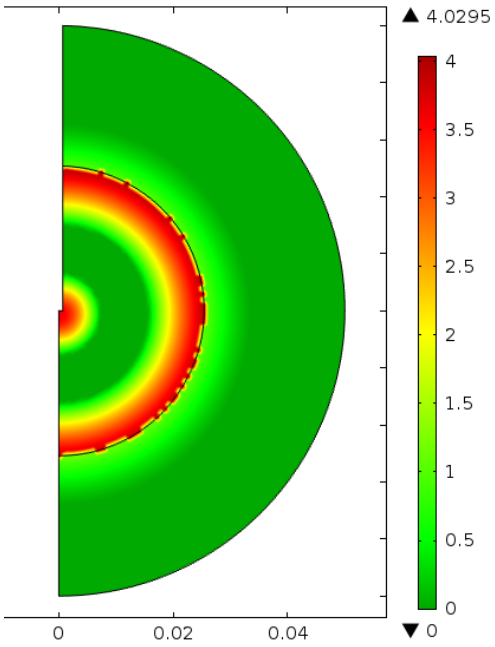

Figure 8: Results of the optimization function after 11.5 minutes of heating. The lower the number, the more optimal the result. Dark green signifies low values, down to zero, which is achieved either by keeping the normal tissue in the 37-38ºC range, or by raising the temperature of the rumor tissue between 43-50ºC. The yellow to red areas indicate tumor tissue outside of this range. The red in the center of the tumor is tissue that has gotten slightly too hot, whereas the yellow, orange and red areas on the outside border of the tumor represent areas that did not reach the optimal 43ºC.

Figure 8 shows that optimal heating (shown in green) occurred in the middle of the tumor and throughout the normal tissue. This indicates that this part of the tumor reached temperatures within the range required for necrosis, and that the normal tissue remained close to 37ºC. The red regions at the center and outer edge of the tumor show that these areas were not in the ideal temperature range for necrosis; in the center, this is due to the tissue becoming too hot, whereas at the outer edge this is due to the tumor not heating enough to cause cell death. However, this tissue is still weakened from the slight heating, and also serves to act as a protective barrier from damage to normal tissue.

The resulting temperature profile at the end of the optimal 11.5 minutes of heating is shown in Figure 9.

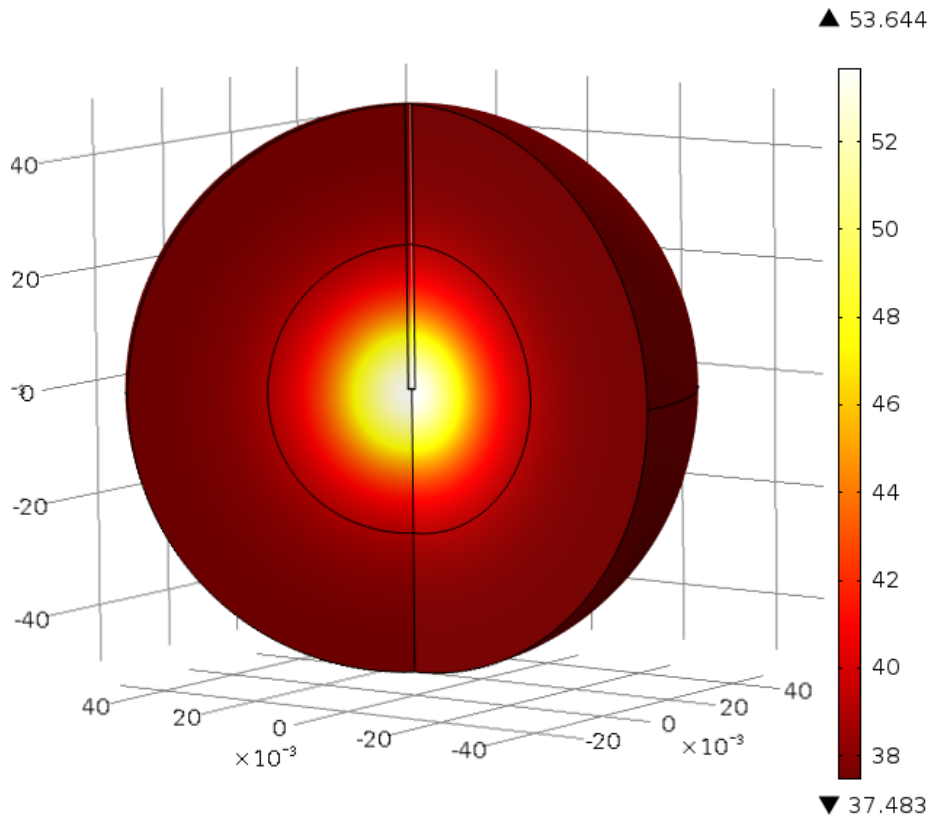

Figure 9: Heat generation profile within the pathogenic tissue at 87,090 seconds (after 11.5 minutes of heating), with bioheat generation throughout the tissue and magnetic heating occurring proportional to nanoparticle concentration.

It can be seen in Figure 9 that the maximum temperature reached for this tumor after 11.5 minutes of heating was 53.5ºC. This is consistent with the red area noted in the optimization function plot in Figure 8. While this technically exceeds the maximum temperature in the optimization model, it is acceptable because it is likely that very little tissue ever reached this temperature and it still remains well below the threshold for thermal ablation of 60°C.

7.5 Necrosis

The amount of tissue that has reached necrosis at the end of the 11.5 minute heating procedure is shown as a plot of CEM43 > 340 minutes in Figure 10; colored areas indicate the portions of tumor that completely necrosed.

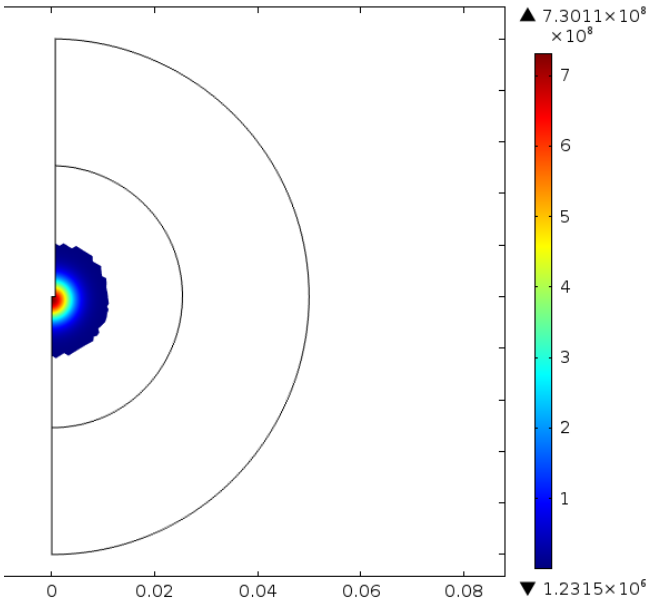

Figure 10: Schema of tumor tissue that underwent necrosis after 11.5 minutes of heating. All colored areas indicate necrosed tissue.

While not all the tissue is necrosed, this does not mean that the procedure was ineffective. Complete necrosis only occurs at the inner parts of the tumor, but this function does not account for tissue that has not quite reached necrosis but has still been damaged. As can bee seen in the temperature profile in Figure 9, the majority of the tumor still experiences significant damage, but stopping treatment before the entire tumor has necrosed also serves to protect the surrounding normal tissue.

It is also worth noting is that this function does not account for temperatures that have gotten too high, such as to cause coagulation, thermal ablation, or charring. While this was not a significant issue for our model with an 11.5 minute heating time, it is a limitation of the model that may be significant at longer heating times or under different conditions.

7.6 Validation

This model was validated in two ways. Initially, comparison to a computational model by Javidi et al. showed that this model followed expected trends. Javidi's model was based on properties of an agarose gel intended to match the properties of a tumor[9]. As seen in Figure 15, increasing flow rate decreases overall heating.

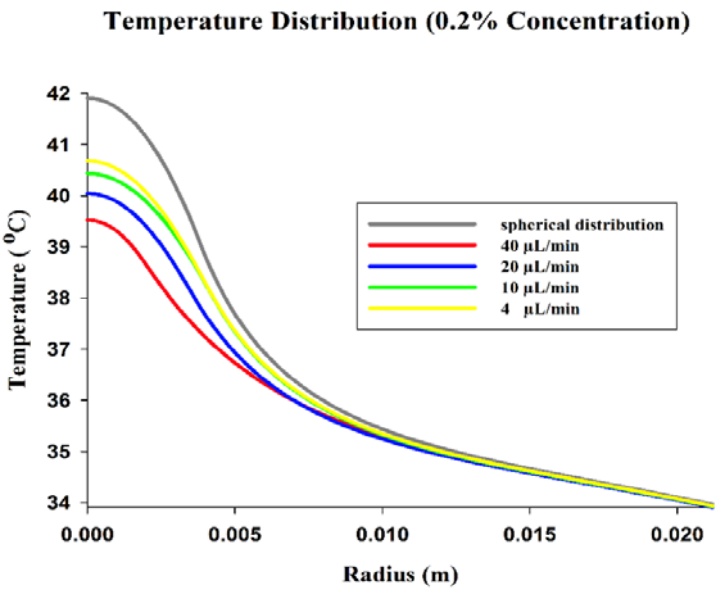

Figure 15: [9] Effect of various flow rates on the overall heating of a tumor with constant properties using magnetic nanoparticle hyperthermia. As the flow rate is increased, overall heating is decreased due to increased dispersion of the magnetic nanoparticles within the tumor.

Javidi's work on the effect of increasing flow rates is validated in this model in Figure 16. In order to recreate Javidi's model, this model's base temperature was readjusted to be 34ºC. A flow rate of 4µL/min was not modeled for comparison, given that to achieve the amount of nanoparticles used in this model, it would take over an hour to inject them at such a slow rate, which is a scenario not relevant to this model.

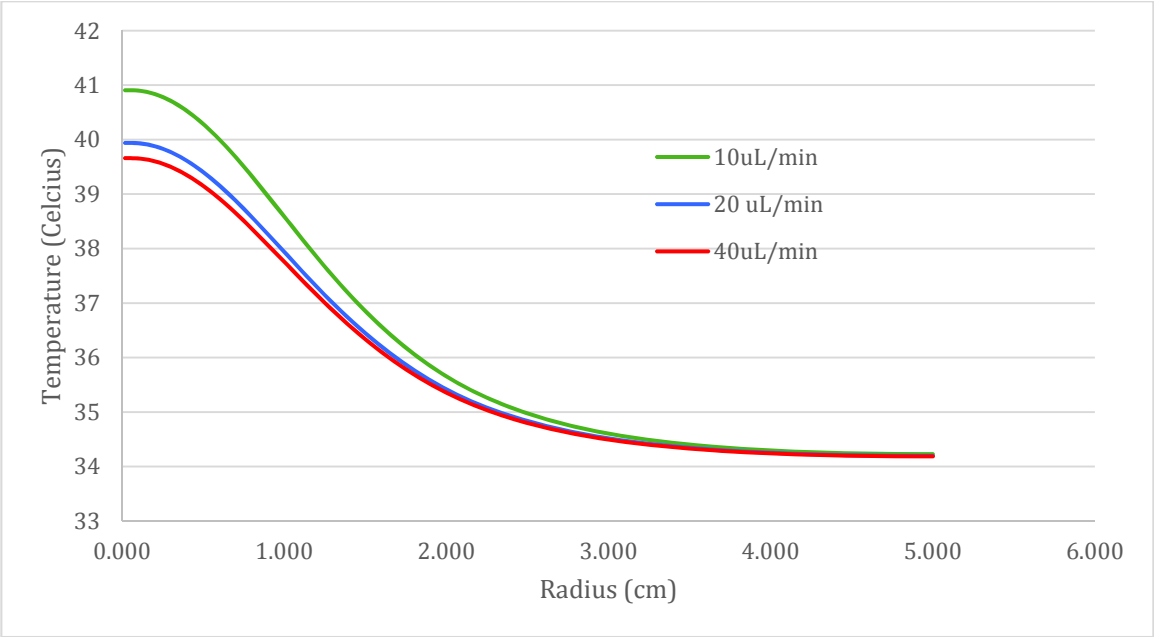

Figure 16: Effect of various flow rates on the overall heating of the spherical tumor with a radius of 2.54cm and initial temperatures set at 34ºC. As the flow rate is increased, overall heating is decreased due to increased dispersion of the magnetic nanoparticles within the tumor, as expected according to Javidi et. al.'s previous research[9].

Additionally, this model was validated with comparison to experiential data. This model was run under the same circumstances that a magnetic nanoparticle hyperthermia experiment was performed on agarose gel with tumor properties by adjusting the model's initial temperature, nanoparticle concentration, and injection time[9]. The results show a high correlation with the experimental data (Figure 17). The model behavior is slightly more linear, potentially because the model does not incorporate changes in tumor properties based on temperature.

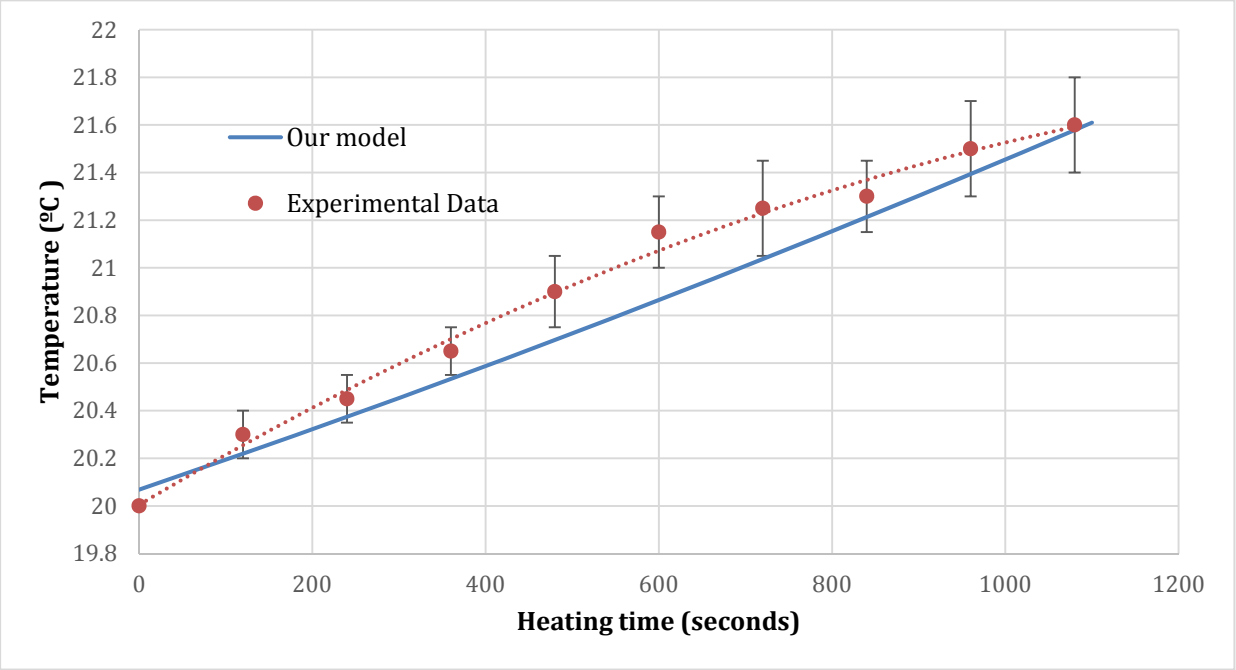

Figure 17: Magnetic nanoparticle hyperthermia experimental results performed in an agarose gel model with tumor tissue properties[9], compared to the same experimental parameters inserted into the computational model and run.

7.7 Sensitivity Analysis

In order to demonstrate the effect of magnetic hyperthermia treatment on different tumor types, sensitivity analysis was performed on various parameters relating to tumor properties, such as diffusivity, porosity, and permeability. Figure 12 shows the sensitivity of final temperature at the center of the tumor with respect to ±10% changes in the parameter values of tumor porosity, thermal conductivity, and heat capacity. Figure 13 shows the sensitivity of final temperature at the center of the tumor with respect to a ±10x change in the parameters of tumor permeability and diffusivity of nanoparticles into the tumor.

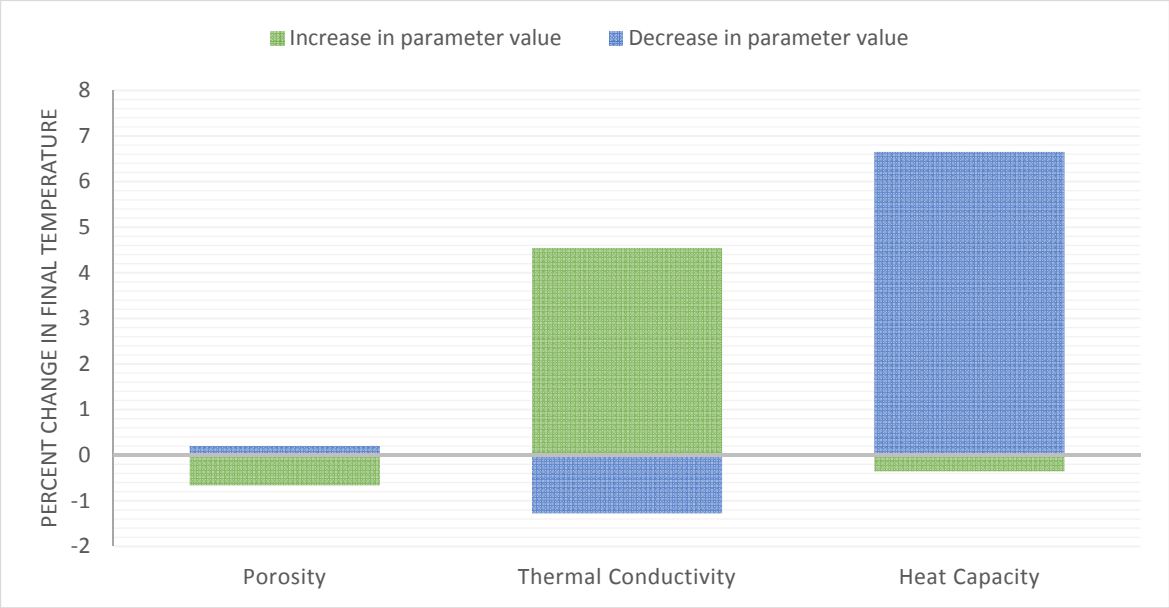

Figure 12: Sensitivity analysis results of various parameters relating to tumor properties varied ± 10% from original values. The original value of tumor porosity is 0.8, the original value of thermal conductivity is 0.55 W/(m*K), and the original value of heat capacity is 4200 J/(kg*K). Percent changes were based on temperatures in Kelvin.

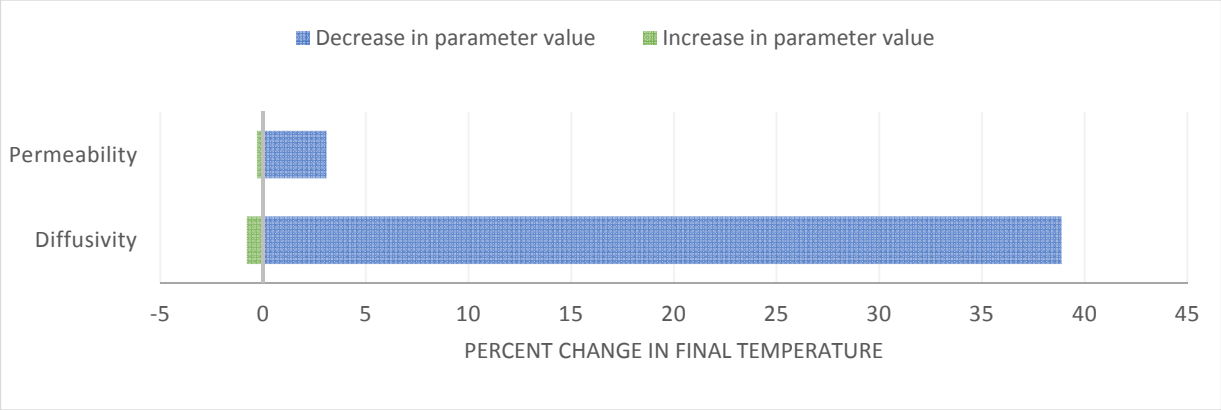

Figure 13. Sensitivity analysis results of the parameters of tumor permeability and diffusivity of nanoparticles into the tumor when varied by a factor of ten. The original value of permeability is 1e-17 m^2, and the original value of diffusivity is 2.5e-10 m^2/sec. Percent changes were based on temperatures in Kelvin.

Figures 12 and 13 show that final temperature at the center of the tumor decreases with increases in porosity, permeability, and diffusivity. This makes sense because all of these properties contribute to creating a more disperse nanoparticle concentration profile, which leads to lower temperatures due to their direct relationship through the electromagnetic heat source term. Diffusivity was further examined in Figure 14. An increase in heat capacity also leads to a lower final temperature because more energy is required to heat the tissue to the same temperature, meaning that for the same amount of heat applied lower final temperature will be reached. In contrast, a decrease in thermal conductivity causes a decrease in final temperature, because there is more resistance to heat transfer.

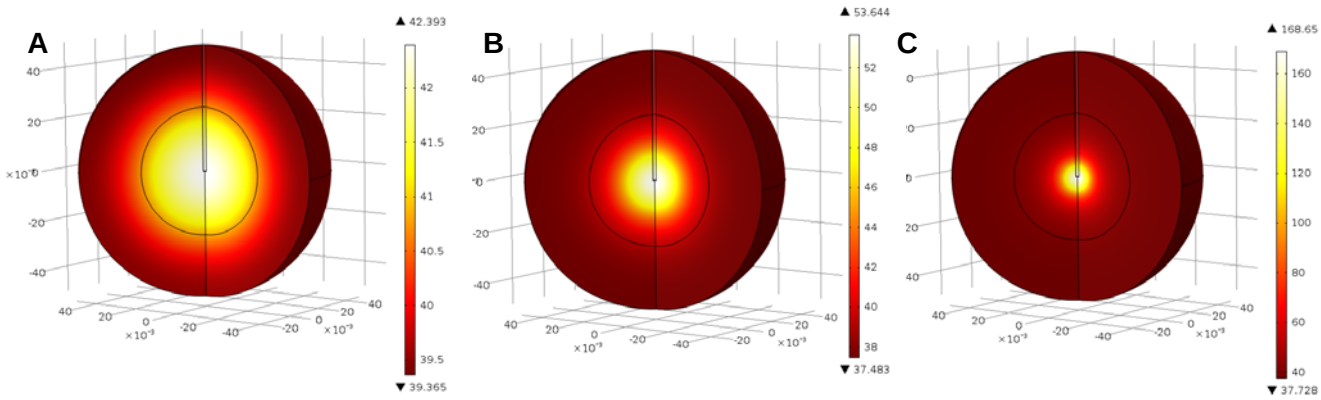

Figure 14. Sensitivity analysis results of tumor diffusivity of nanoparticles into the tumor when varied by a factor of ten. The original value of diffusivity, the results of which are shown in (b), is 2.5e-10 m^2/sec. The results using a higher diffusivity (2.5e-9 m^2/sec) are shown in (a), and the results using a lower diffusivity (2.5e-11 m^2/sec) are shown in (c).

Figure 14 shows temperature profiles at the final time resulting from changes in diffusivity by a factor of ten. It can be seen that increasing diffusivity of the nanoparticles in the tissue results in a more disperse temperature profile with a lower maximum temperature of 42.4°C. This is in contrast to a decrease in diffusivity, which results in a more localized temperature distribution with a much higher maximum temperature of 168.7°C. This is because at a higher diffusivity, nanoparticles will diffuse farther out into the tissue, resulting in a more spread out concentration profile, and therefore lower overall temperatures. At a lower diffusivity, nanoparticles cannot move as far away from injection site, resulting in a tightly packed, highly concentrated sphere of nanoparticles. Because they are at such high concentration, this will result in much higher temperatures reached only at the center of the tumor. Increasing diffusivity has a much more dramatic affect on percent change in final temperature than decreasing diffusivity by the same factor. This is because when diffusivity is increased and the maximum temperature reached decreases, there is a lower boundary of body temperature that limits the percent change in the final temperature that can be achieved.

Overall, final temperature is shown to be most sensitive to a decrease in diffusivity compared to changes in other properties. However, because diffusivity is a property of both the tissue and type of nanoparticle, this property can be most easily controlled by varying the type of nanoparticle used.

8.0 Conclusions and Future Directions

This model accurately coupled our three physical processes together. Injection was modeled as a mass flux boundary at the needle tip, and injection time was calculated to be 15 minutes in order to inject 300 μL of nanoparticle fluid into the tumor at 20 μL/min. This then created a Darcy velocity profile that was

used as the convective velocity in the mass transfer process. Our model allows the nanoparticles to diffuse within the tumor for 24 hours, before then applying the magnetic field. This accurately reflects the current clinical procedures and trials being performed by allowing the nanoparticles time to diffuse out, and therefore heat the tumor more uniformly. Heat generation was then successfully implemented as a function of nanoparticle concentration, and an optimal heating time based on specific tumor and nanoparticle properties was determined to be 11.5 minutes. In most previous research, the heat generation was calculated using an exponential decay function from the site of injection[6,12], but allowing our model to incorporate a heating term based on concentration profile made it more accurate.

Tissue necrosis was calculated using cumulative equivalent minutes at 43ºC. Using this method, it was found that at a heating time of 11.5 minutes a portion of the center of the tumor was completely necrosed. While not all tumor tissue was destroyed, temperature profiles indicate that all the tumor tissue was at least heating above body temperature, while all normal tissue remained around body temperature. This fit our goal of damaging tissue enough to make it more susceptible to other treatments, but the model could also be adjusted based on this function if more tissue destruction was desired.

This model was validated through comparison to other computer models as well as experimental data. These comparisons confirmed that our model was accurate and that all involved physics had been correctly implemented in COMSOL. Comparison to experimental data also indicates that our model is an accurate representation of an experimental tumor model and confirms that it could be useful in the future to predict how treatments will affect various tumor types.

Sensitivity analysis on tumor-related properties indicated that final temperature reached is most influenced by the diffusivity of nanoparticles in the tumor. The electromagnetic heat generation is directly related to the concentration profile of nanoparticles, which is highly dependent on diffusivity. This indicates that the type of nanoparticle used will have a large effect on the amount of heat generated, which is an important point for consideration in designing patient-specific treatments. Much of the current research on the use of magnetic hyperthermia for tumor treatment is focused on the design of new nanoparticles and their properties[10]. Our model can be employed to test the various properties of these nanoparticles as they are created, and optimize them for use in hyperthermia treatments.

There are many potential future directions this work could lead to. In addition to adjusting our model to reflect different nanoparticle properties, future applications include changing the model to reflect different tumor properties and geometries, testing and implementing parameters that change with temperature, and modeling more than one injection site. We could also potentially optimize combinations of heating time and electromagnetic fields applied, as well as test different types of heating, such as ultrasound or microwave. The flexibility of this model to be able to give accurate results for different input parameters allows for prediction of the affect of magnetic hyperthermia on different tumor types, which could allow for patient-specific treatment design and optimization.

9.0 Appendix

9.1 Mesh Convergence

In order to determine the minimum number of mesh elements necessary to achieve as accurate a solution as possible, a mesh convergence was completed. This was done by doing a parametric sweep on the maximum element size of the user defined mesh and evaluated temperature after 88,200 seconds (after 24 hours of diffusion and 30 minutes of heating) at the point r = 0.001m, z = 0.002, a point slightly below the tip of the needle. Maximum element sizes of 0.07, 0.0462, 0.028, 0.0014, and 0.0007 were used. The variable of temperature was chosen for the mesh convergence because the temperature is ultimately what will define the extent of tissue necrosis. The results of the mesh convergence are shown in Figure 11. It can be seen that as maximum element size decreases, the temperature at the point converges to around 360 K, or 87ºC.

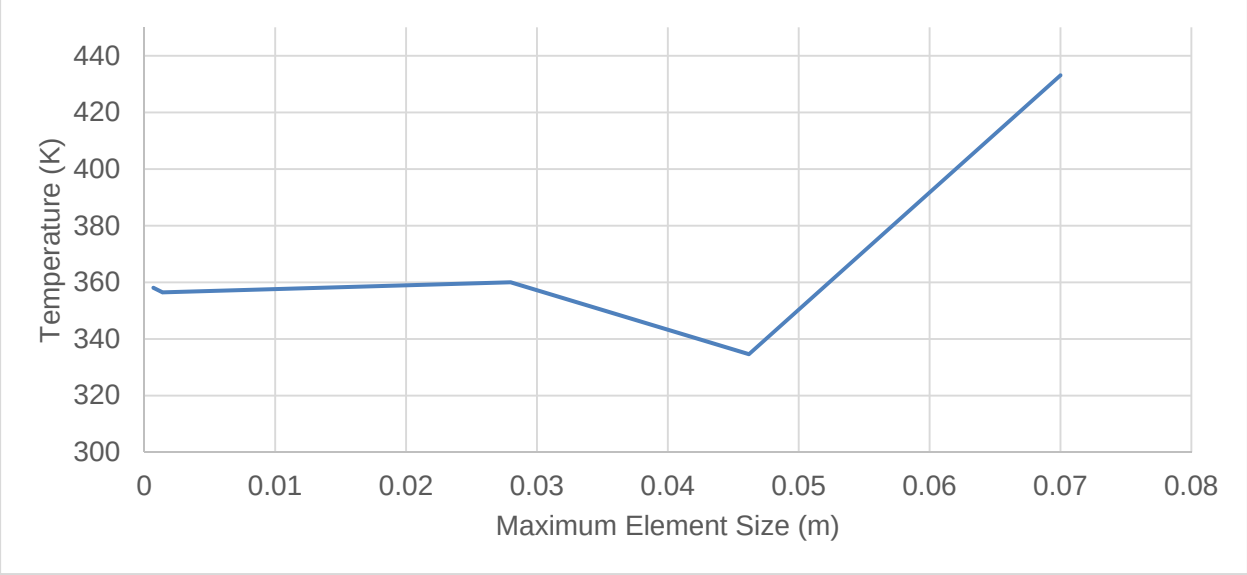

Figure 11: Temperature at point (r,z) = (0.000343m, -0.001m) vs. maximum mesh element size.

Figure 11 show that temperature converges around a maximum element size of 0.028. However, overall temperature variation shown is only within about 2 K, and since this mesh convergence was performed across the entire range of mesh sizes, it can be concluded that the mesh does not have a significant effect on the solution. Since computation time was not an issue, a maximum element size of 0.0014 m, with element size 0.001m at the needle tip and left tumor boundary, was used for all further computation.

9.2 Parameter values

Table 1: User-defined approximated input parameters for Darcy pressure-driven flow of the nanoparticle fluid out of the syringe and into the malignant tumor.

Parameter	**Symbol**	**Value**	**Source**
Nanoparticle Fluid Density	ρ	1011.85 kg/ m^3	Javidi; [9]
Nanoparticle Fluid Dynamic Viscosity	μ	0.001 Pa/s	Javidi; [9]
Tumor Porosity	ϵ_p	0.8	Audigier, Sciume; [21,22]
Tumor Permeability	κ	1 e-17 m^2	Audigier; [21]

Table 2. Parameter values used for nanoparticle concentration profile calculation

Parameter	**Symbol**	**Value**	**Source**
Diffusivity of particles into tissue	$D_{NP,tissue}$	2.5e-10 m^2/s	Golneshan; [2]

Table 3. Parameter values used for calculation of heat generation in a tumor with bioheat and magnetic heat sources.

Parameter	**Symbol**	**Value**	**Source**
Tissue density	ρ_{tumor}	1000 kg/ m^3	Salloum; [23]
Tissue thermal conductivity	k	0.55 W/m*K	Salloum; [23]
Tissue specific heat	c_p	4200 J/kg*K	Salloum; [23]
Volumetric blood flow rate through tissue	$\dot{V}_b^v$	5 x 10^{-4} s^{-1}	Salloum; [23]
Blood specific heat	$c_{p\ b}$	3639 J/kg*K	Kim; [24]
Blood density	ρ_b	1060 kg/ m^3	
Arterial blood temperature	T_a	310.15 K	
Permeability of free space	μ_o	4 π x 10^{-7} N/A^2	Javidi; [9]
Amplitude of magnetic field	H_o	1.2 kAm^{-1}	Javidi; [9]
Frequency of magnetic field	f	164 kHz	Javidi; [9]
Nanoparticle fluid viscosity	η	0.001 Pa•s	Javidi; [9]
Average relaxation time in response to thermal fluctuation	τ_o	10 x 10^{-9} s	Javidi; [9]
Domain Magnetization	M_d	4.46 x 10^8 Gauss	Javidi; [9]
Boltzmann constant	k	1.38 x 10^{-23} J/K	Javidi; [9]
Magnetocrystalline anisotropy constant	K	9 kJ/m^3	Javidi; [9]
Nanoparticle diameter	D	8 nm	Javidi; [9]
Nanoparticle density	ρ_{NP}	5.24 x10^6 g/m^3	Javidi; [9]
Nanoparticle heat capacity	$c_{p,NP}$	670 J/(kg•K)	Javidi; [9]
Ligand layer thickness	δ	1 x 10^{-9} m	Javidi; [9]

9.3 Team Responsibilities Form

Team member name	Member1: Sonja	Member2: Samantha	Member3: Alexa	NOT DONE
Wrote abstract		X	X	
Edited abstract	X	X	X	
Wrote introduction	X			
Edited introduction	X	X	X	
Wrote method section	X	X	X	
Edited method section	X	X	X	
Wrote results section	X	X	X	
Edited results section	X	X	X	
Wrote discussion section	X	X	X	
Edited discussion section	X	X	X	
Wrote summary and conclusion section	X	X	X	
Edited summary and conclusion section	X	X	X	
Wrote bibliography section	X	X	X	
Edited bibliography section	X	X	X	
Prepared processed data table for appendix	X	X	X	
Checked data in processed data table in appendix	X	X	X	
Prepared figures or tables for main text	X	X	X	
Checked figures or tables in main text	X	X	X	
Assigned tasks to group members	X	X	X	
Put the report together from the parts provided by others	X	X	X	
Read and edited entire document to check for consistency	X	X	X	

10.0 References

[1] S. Dutz and R. Hergt, “Magnetic particle hyperthermia – a promising tumour therapy?” *Nanotechnology,* vol. 25 no. 45, pp. 1-28, 2014.

[2] A. Golneshan and M. Lahonian, 'Diffusion of magnetic nanoparticles in a multi-site injection process within a biological tissue during magnetic fluid hyperthermia using lattice Boltzmann method', *Mechanics Research Communications*, vol. 38, no. 6, pp. 425-430, 2011.

[3] A. Attaluri, S. Kandala, M. Wabler, H. Zhou, C. Cornejo, M. Armour, M. Hedayati, Y. Zhang, T. DeWeese, C. Herman and R. Ivkov, 'Magnetic nanoparticle hyperthermia enhances radiation therapy: A study in mouse models of human prostate cancer', *International Journal of Hyperthermia*, pp. 1-16, 2015.

[4] J. Hainfeld, L. Lin, D. Slatkin, F. Avraham Dilmanian, T. Vadas and H. Smilowitz, 'Gold nanoparticle hyperthermia reduces radiotherapy dose', *Nanomedicine: Nanotechnology, Biology and Medicine*, vol. 10, no. 8, pp. 1609-1617, 2014.

[5] A. Deatsch and B. Evans, 'Heating efficiency in magnetic nanoparticle hyperthermia', *Journal of Magnetism and Magnetic Materials*, vol. 354, pp. 163-172, 2014.

[6] A. Golneshan and M. Lahonian, 'The effect of magnetic nanoparticle dispersion on temperature distribution in a spherical tissue in magnetic fluid hyperthermia using the lattice Boltzmann method', *International Journal of Hyperthermia*, vol. 27, no. 3, pp. 266-274, 2011.

[7] J. Hainfeld and Huang, 'Intravenous magnetic nanoparticle cancer hyperthermia', *IJN*, p. 2521, 2013.

[8] T. Kobayashi, 'Cancer hyperthermia using magnetic nanoparticles', *Biotechnology Journal*, vol. 6, no. 11, pp. 1342-1347, 2011.

[9] M. Javidi, M. Heyardi, A. Karimi, M. Haghpanahi, M Navidbakhsh, and A. Razmkon, “Evaluation of the effects of injection velocity and different gel concentrations on nanoparticles in hyperthermia therapy,” *Journal of Biomedical Physics and Engineering,* vol. 4 no. 4, pp. 151-162, 2014.

[10] C.S. Kumar, and F. Mohammad, “Magnetic nanomaterials for hyperthermia-based therapy and controlled drug delivery,” *Adv. Drug. Deliv Rev,* vol. 63, pp. 789-808, 2011.

[11] S. Deger, D. Boehmer, I. Turk, J. Roigas, V. Budach, S.A. Loening, “Interstitial hyperthermia using self-regulating thermoseeds combined with conformal radiation therapy,” *Eur. Urol,* vol. 42, ppg. 147-153, 2002.

[12] M. Salloum, R. Ma, D. Weeks and L. Zhu, 'Controlling nanoparticle delivery in magnetic nanoparticle hyperthermia for cancer treatment: Experimental study in agarose gel', *International Journal of Hyperthermia*, vol. 24, no. 4, pp. 337-345, 2008.

[13] C. Koch and A. Winfrey, 'FEM Optimization of Energy Density in Tumor Hyperthermia Using Time-Dependent Magnetic Nanoparticle Power Dissipation', *IEEE Transactions on Magnetics*, vol. 50, no. 10, pp. 1-7, 2014.

[14] I. Astefanoaei, I. Dumitru, A. Stancu and H. Chiriac, 'A thermo-fluid analysis in magnetic hyperthermia', *Chinese Phys. B*, vol. 23, no. 4, p. 044401, 2014.

[15] A. Jordan, R. Scholz, K. Maier-Hauff, M. Johannsen, P. Wust, J. Nadobny, H. Schirra, H. Schmidt, S. Deger, S. Loening, W. Lanksch and R. Felix, 'Presentation of a new magnetic field therapy system for the treatment of human solid tumors with magnetic fluid hyperthermia', *Journal of Magnetism and Magnetic Materials*, vol. 225, no. 1-2, pp. 118-126, 2001.

[16] F. Di Michele, G. Pizzichelli, B. Mazzolai, and E. Sinibaldi, "On the preliminary design of hyperthermia treatments based on infusion and heating of magnetic nanofluids," *Mathematical Biosciences,* vol. 262 no. 2015, pp. 105-116, 2014.

[17] M.W. Dewhirst, B.L Vigilanti, M. Lora-Michiels, M. Hanson, and P.J. Hoopes, "Basic principles of thermal dosimetry and thermal thresholds for tissue damage from hyperthermia," *Int. J. Hyperthermia,* vol. 19 no. 3, pp. 267-294, 2003

[18] F.K. Storm, W.H. Harrison, R.S. Elliott, D.L. Morton, "Normal tissue and solid tumor effects of hyperthermia in animal models and clinical trials," *Cancer Research,* vol. 39, pp. 2254-2251, 1979.

[19] S.A. Separerto, and W.C. Dewey, "Thermal dose determination in cancer therapy," *International Journal of Radiation Oncology*Bioloty*Physics*, vol. 10 no. 6, pp. 787-800, 1984.

[20] I. Chang, "Considerations for thermal injury analysis for FR ablation devices, *The Open Biomedical Engineering Journal,* vol. 4 no. 1, pp. 3-12, 2010.

[21] C. Audigier, T. Mansi, H. Delingette, S. Rapaka, V. Mihalef, D. Carnegie, E. Boctor, M. Choti, A. Kamen, D. Comaniciu, et al, "Parameter Estimation For Personalization of Liver Tumor Radiofrequency Ablation," *Computational and Clinical Applications,* 2014.

[22] G. Sciumè, R. Santagiuliana, M. Ferrari, P. Decuzzi and B. Schrefler, 'A tumor growth model with deformable ECM', *Phys. Biol.*, vol. 11, no. 6, p. 065004, 2014.

[23] M. Salloum, "Enhancement in treatment planning for magnetic nanoparticle hyperthermia: Optimization of the heat absorption pattern," *J Hyperthermia,* vol. 25 no. 4, pp. 309-321, 2009.

[24] B. Kim, G. Han, B. Toley, C.K. Kim, V. Rotello, and N. Forbes, "Tuning payload delivery in tumour cylindroids using gold nanoparticles," *National Nanotechnology,* vol. 5 no. 6, pp. 465-472, 2010.